Research article

# Ozone structure in Caribbean hurricanes

Mark R. Jury [a,b,*], Ivan L. Fontanez-Vazquez [a]

[a] *Physics Dept, University of Puerto Rico Mayagüez, 00681 USA*
[b] *University of Zululand, KwaDlangezwa, 3886 South Africa*

## ARTICLE INFO

## ABSTRACT

Using ozone data from model-assimilated satellite measurements in the eastern Caribbean 15–20N, 60–68W, cases were studied when upper tropospheric O3 values declined below 60 ppb. Secondary criteria on convection and circulation isolated two hurricanes for analysis (Irma and Maria 2017). Winds at 150 hPa (14 km) show divergence over the vortex characterized by ozone <50 ppb. Upper tropospheric O3 concentrations >100 ppb appear west of hurricanes, where sinking motions interact with vortex outflow. Past work suggests that high values are important, but here low ozone concentrations near the core are more conspicuous. The low O3 layer formed over the ocean and lifted by the hurricane circulation and convection, indicates vortex – environment interaction, vertical motion and storm intensity. Upper tropospheric O3 concentrations <50 ppb cover an area about double the radius of heavy rainfall >10 mm/h, appearing as a protective envelope around the core.

## 1. Introduction

Tropospheric ozone (O3) is a greenhouse gas and a precursor of hydroxyl. Its generation involves photochemical oxidation of carbon monoxide and volatile organic compounds in the presence of nitrogen oxides (Zhang et al., 2010). Tropospheric ozone sources are typically located over land and include biomass burning, industrial and transportation emissions, lightning and soil decomposition (Ryu and Jenkins 2005; Jenkins et al., 2015). The oceans act as a sink, due to chemical destruction of O3 by halogens in the marine layer (Read et al., 2008; Saiz-Lopez and Fernandez 2016), particularly over sub-tropical upwelling plumes (Reid et al., 2009). Tropospheric O3 increases with height from 20 to 200 parts per billion (ppb) depending on proximity to pollution sources (Logan 1999). Ozone exceeds 1000 ppb in the stratosphere (McPeters et al., 2007), yet chemical transformation near the surface often prevails over stratospheric influx (Prather and Ehhalt 2001).

Ozone measurements by satellite radiometers using backscattered ultra-violet emissions (SBUV) since 1979 contained uncertainties in tropospheric versus stratospheric components (Ziemke et al., 2006). More recently multi-spectral infrared radiometers (eg. AIRS, IASI, cf. Table 1) have enabled O3 profiles at ~ 1 km resolution (Monahan et al., 2007; Boynard et al., 2009; Cuesta et al., 2013). Validation studies with ozone-sondes and GPS refractometers have revealed accurate spatial and temporal patterns (Zhang et al., 2010) that contributed to meteorological air-chemistry model assimilation errors <10% (Wargan et al., 2017).

These efforts underpin our understanding of atmospheric controls on tropospheric ozone concentrations.

Convective waves that intensify into tropical cyclones (TC) tend to produce low ozone concentrations in the upper troposphere due to the rising of marine air around the eye-wall (Zou and Wu 2005; Cairo, 2008; Jenkins et al., 2015). Carsey and Willoughby (2005) report ozone measurements during aircraft transects of Atlantic hurricanes that show corresponding fluctuations of O3 and vertical motion. Strong O3 gradients around the eye-wall were measured for intensifying TC in contrast with weakening cases with relatively uniform distribution. Tropospheric ozone depletion during TC passage over Madagascar (Jury 2016) suggests O3 as an important tracer of vertical motion.

Jang et al. (2003), Wu and Zou (2008), and Liu and Zhang, 2016 assimilated satellite total column ozone fields and found improved storm forecasts. Zou and Wu (2005) observed that the spatial distribution of total ozone within TCs correlated with vorticity and upper-level geopotential height. Incorporating AIRS ozone profiles in hurricane simulations, Liu and Zou (2015) found that mid-tropospheric convective heating rose 5C and near-surface winds increased 10 m/s.

The Modern-Era Retrospective analysis for Research and Applications (MERRA-2) meteorological reanalysis (Molod et al., 2015, Gelaro et al., 2017; Orbe et al., 2017) describes daily ozone concentrations at ~0.5° horizontal and ~0.5 km vertical resolution. In addition to satellite data assimilation, MERRA-2 includes emission inventories, satellite fire and lightning detection, parameterized land surface and air chemistry

---

**Table 1.** List of satellites measuring tropospheric ozone.

| Year | Platform | Sensors |
|---|---|---|
| 1978- | Nimbus-7 | LIMS limb scanner, TOMS-1, SBUV |
| 1991- | Meteor-3 | TOMS-2 (UV back-scattering) |
| 1995- | ERS-2 | GOME-1 (SBUV type) |
| 1996- | TOMS-EP | TOMS-3, SBUV/2 |
| 2002- | Envisat | SCIAMACHY |
| 2002- | MODIS | AIRS (IR absorption) |
| 2004- | EOS-Aura | OMI-SBUV/2, MLS- TES- limb scanner |
| 2006- | MetOp-A | GOME-2, IASI (IR interferometer) |
| 2012- | MetOp-B | GOME-2, IASI |
| 2017- | Sentinel-5 | TROP-OMI |
| 2018- | MetOp-C | GOME-2, IASI |

The following websites provide acronyms and further details: http://rammb.cira.colostate.edu/dev/hillger/ozone-monitoring.htm; https://ozonewatch.gsfc.nasa.gov/; https://wdc.dlr.de/sensors/.

transformation, and mass flux closure (Knowland et al., 2017; Ziemke et al., 2019). Model vertical motion is said to be constrained by satellite O3 measurements. Here in this brief study, MERRA-2 ozone and wind fields describe the vertical structure around hurricanes in the eastern Caribbean, and provide results that contrast with past research (Das et al., 2016).

## 2. Data and methods

Given the availability of multiple satellites providing vertical profiles of tropospheric ozone (Pittman et al., 2009; cf. Table 1), we confine our study to the period 2005–2017. During preliminary analysis, 150 hPa was found to be a sensitive level where low ozone signatures can be detected in a layer normally high in ozone. O3 monitoring at that elevation (~14 km) benefits from additional satellites intended for stratospheric retrievals. To limit the effects of intermittent satellite data and cloud-screening, the MERRA-2 daily minimum 150 hPa ozone value was obtained within the eastern Caribbean: 15–20N, 60–68W, hereafter the O3 index. Similarly, daily maximum values were obtained for

MERRA-2 925 hPa wind vorticity and 150 hPa divergence, and cMorph satellite rainfall (Joyce et al., 2004). Hence we track a $50 \times 50$ km signal within the $500 \times 800$ km eastern Caribbean area in the period 2005–2017. Intercomparison of daily minimum 150 hPa AIRS satellite and MERRA-2 ozone values in the eastern Caribbean (Appendix: Figure A1) reveal sufficient agreement ($r^2 = 0.60$) but there is some bias above 100 ppb (satellite > model). To provide context, we calculate the mean ozone profile 2005–2017 on 17N latitude at a point east of Puerto Rico (65W) and west of Dakar, Senegal (20W).

A ranking hierarchy was applied to all daily time series: 1) 150 hPa O3 index $<60$ ppb, 2) rain-rate $>10$ mm/day, 3) 925 hPa vorticity $>10^{-4}$ $s^{-1}$ and 4) 150 hPa divergence $>10^{-4}$ $s^{-1}$. With these multiple ranking criteria, 29 cases were identified in late summer (cf. Table 2).

Cross-correlations were calculated between the O3 and meteorological indices, for continuous data and for the 29 cases meeting the above criteria. Point-to-field correlations were analyzed between the O3 index and fields of continuous sea level air pressure N = 4747 and Jul–Oct satellite net outgoing longwave radiation (OLR) N = 1582.

**Table 2.** Ranking hierarchy (right) and cases meeting the criteria: ranked by 150 O3. Values are min (ozone) or max weather values within the eastern Caribbean area (cf. Figure 1b). Asterisks refer to TC cases presented.

| date | 150 O3 | Rainfall | 925 vort | 150 div |
|---|---|---|---|---|
| *6-Sep-17 | 44.45 | 42.10 | 4.76 | 2.66 |
| 7-Sep-17 | 46.45 | 13.92 | 1.49 | 1.52 |
| *19-Sep-17 | 47.62 | 41.79 | 3.30 | 1.90 |
| 23-Aug-12 | 49.12 | 19.86 | 3.93 | 2.55 |
| 21-Sep-17 | 50.07 | 13.47 | 1.30 | 1.32 |
| 20-Sep-17 | 50.13 | 48.32 | 4.30 | 2.39 |
| 15-Oct-08 | 50.95 | 41.07 | 1.65 | 2.22 |
| 31-Aug-10 | 51.07 | 13.21 | 1.75 | 1.23 |
| 30-Aug-10 | 51.15 | 50.25 | 4.29 | 2.35 |
| 22-Aug-11 | 51.35 | 27.22 | 2.77 | 1.63 |
| 18-Aug-07 | 51.40 | 21.25 | 1.40 | 1.03 |
| 13-Oct-12 | 51.41 | 36.08 | 3.15 | 1.87 |
| 11-Sep-11 | 52.39 | 43.62 | 2.86 | 1.79 |
| 4-Oct-10 | 52.45 | 27.66 | 2.80 | 1.88 |
| 16-Oct-08 | 52.47 | 44.25 | 3.26 | 2.37 |
| 3-Aug-11 | 53.39 | 24.76 | 1.07 | 1.03 |
| 5-Oct-10 | 53.42 | 33.42 | 2.80 | 1.69 |
| 6-Oct-10 | 53.44 | 33.81 | 1.27 | 1.73 |
| 21-Sep-08 | 53.74 | 44.09 | 1.39 | 1.76 |
| 14-Oct-12 | 55.08 | 32.88 | 3.64 | 1.91 |
| 2-Aug-11 | 55.66 | 16.01 | 2.04 | 1.65 |
| 12-Sep-11 | 55.89 | 22.82 | 1.33 | 1.81 |

**Ranking hierarchy:**1) min 150 hPa O3 < 60 ppb; 2) max rain >10 mm/day; 3) max 925 hPa vort >$10^{-4}$ $s^{-1}$; 4) max 150 hPa div >$10^{-4}$ $s^{-1}$.

We evaluated maps of 150 hPa O3 for the 29 cases and screened out linear patterns, retaining those with circular-shape. Subsequent inspection of meteorological maps and ozone sections yielded a repetitive pattern, and hurricanes Irma and Maria 2017 were selected for analysis. The maps and vertical sections provide information about advection and entrainment around the hurricane, but with 50 km resolution MERRA-2 cannot resolve the eye itself. Therefore, data on convective intensity was employed, including cMorph rainfall and Cloudsat reflectivity. Knowland et al. (2017) describe minor discrepancies in the MERRA-2 model representation of tropospheric ozone, and conclude that results are sufficiently robust to warrant a degree of confidence, despite satellite radiometer O3 response functions that tend to maximize over the ocean above 700 hPa (Cuesta et al., 2013).

## 3. Results

Figure 1a-d illustrates the O3 index time series, eastern Caribbean area, mean annual cycle and mean Jul–Oct O3 profiles. Temporal fluctuations reveal an episodic character that is generally higher in early summer and lower during late winter, similar to Read et al. (2008). Peaks in early summer refer to stratospheric injection of high O3 associated with tropopause folding near cut-off lows (Langford et al., 1996). Late summer minima are of interest here, when daily values of O3 decline below 60 ppb in the presence of a TC circulation. In the absence of TC,

low ozone air in the marine layer seldom reaches the 150 hPa level. The mean profile of ozone over the Caribbean is quite similar to that found near the coast of West Africa (Figure 1d), with values rising gradually from 40 ppb to 120 ppb from 1000 to 200 hPa. In the layer around 150 hPa ozone concentrations rise quickly, exceeding 200 ppb by 100 hPa.

Table 3a,b lists the pair-wise correlation of continuous and case-study ozone values. The O3 index correlates negatively with maximum rainfall and 925 hPa vorticity in the eastern Caribbean in continuous time series N = 4747, but the association with 150 hPa divergence is weak. During late summer events, the O3 correlation with all three weather variables strengthens < -0.451 (N = 29).

Figure 1e,f shows the point-to-field correlation of the O3 index onto fields of sea level air pressure and satellite net OLR in late summer (Jul–Oct). Higher pressure and reduced convection (+OLR) are associated with increased 150 hPa ozone concentrations, as expected. The continuous pressure correlation extends toward South America and the equatorial Atlantic, while the seasonal OLR correlation remains in the eastern Caribbean.

## 4. Hurricane Irma and Maria 2017

Hurricanes Irma and Maria passed through the northeastern Antilles at category 5 intensity on 6 and 19 September 2017 (Cangialosi et al., 2018; Pasch et al., 2018), producing great destruction. Radiosonde
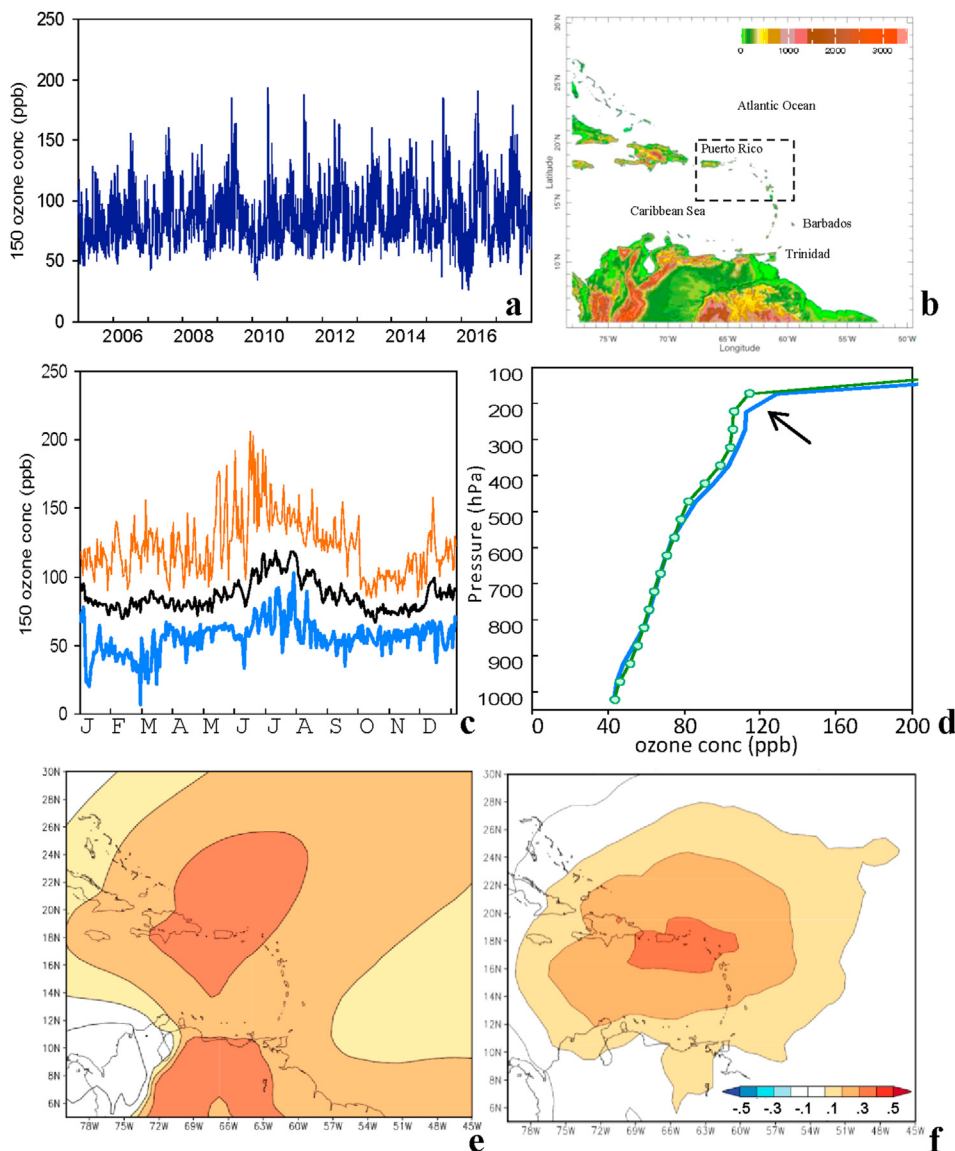


**Figure 1.** (a) Daily minimum 150 hPa ozone time series; (b) eastern Caribbean and index area (dashed) with elevation; (c) mean annual cycle of daily minimum 150 O3 and its upper and lower 2.5 percentiles; (d) mean profiles of O3 averaged Jul–Oct season at 17N, 20W (near Africa, line with dots) and 17N, 65W (Caribbean), arrow points to the 150 hPa value. Point-to-field correlation of the O3 index onto: (e) continuous sea level air pressure N = 4747 and (f) Jul–Oct net outgoing longwave radiation N = 1582.

**Table 3.** Pair-wise cross-correlation of daily data: (a) continuous N = 4747, and (b) only cases listed in Table 1 (N = 29).

| (a) | 150 O3 | Rainfall | 925 vort |
|---|---|---|---|
| Rainfall | -0.154 | | |
| 925 vort | -0.120 | 0.470 | |
| 150 div | 0.019 | 0.522 | 0.353 |
| (b) | 150 O3 | Rainfall | 925 vort |
| Rainfall | -0.451 | | |
| 925 vort | -0.529 | 0.648 | |
| 150 div | -0.461 | 0.663 | 0.793 |

profiles at Guadeloupe and Puerto Rico measured CAPE ~3000 J/kg in the pre-storm environments. The ozone sections on 6 and 19 September 2017 (Figure 2a, Figure 3a) reveal a column of low concentrations from 1000 to 400 hPa of 200 km width. Higher O3 values are found on the upper west side of Irma and to less extent Maria, and pinch the low ozone column in the 300–200 hPa layer. The 925 hPa cyclonic winds and 150 hPa divergent flow (Figure 2b,d and Figure 3b,d) lift low ozone air to the tropopause. The 150 hPa O3 minimum extended southeast, while upper divergence was mainly northwestward. There was low ozone to NW and high ozone to NE of hurricane Maria due to tropical and extratropical cyclones, respectively. Both hurricanes exhibited upper anticyclonic flow around the ozone minimum.

The meridional wind sections (Figures 2c, 3c) sharply divide the west/front and east/back sides of the TC. Because of the latitude extent of these circulation regimes (~10°), vertical motions may be generated according to (Holton 1992): W = V(Z)(β/f), where W is vertical motion, V ~20 m/s, Z ~10 km depth, β = df/dy ~1.5 $10^{-11}$ $s^{-1}$, f ~4.5 $10^{-5}$ $s^{-1}$, assuming steady vorticity advection. W is of order 0.05 m/s, and downward (upward) to the west (east) of TC. Thus high ozone air near the tropopause subsides in front of hurricanes, and low ozone air from the marine layer lifts behind the vortex.

Supplementing the case study 'snapshots', we consider the evolution and westward propagation of the 150 hPa ozone signal in a week-long hovmoller plot (Figure 4a). Hurricane Irma intensified around 50W, and its low ozone feature had a 600 km width and propagated at 6 m/s. The high ozone features west/east of the TC were intermittent, and displaced ~800 km from the axis of low O3.

The hovmoller plot reveals a satellite rain-rate > 5 mm/h along a narrow swath of ~200 km, consistent with the hurricane eye-wall and its convective heating. We infer the low ozone feature delineates the radial extent of rising air in spiral bands feeding the TC perimeter, where deep thermodynamically rich air (CAPE >2000 J/kg) shields the inner core from dry air entrainment.

Convective rainfall in hurricane Irma was confined to the inner vortex <400 km diameter (Figure 4b). Rain rates of ~25 mm/h suggest mid-tropospheric heating anomalies of 8C. The envelope of upward motion covers the circular area of low ozone ~800 km diameter that is quite symmetrical in Irma. The Cloudsat section on 6 Sep 2017 (Figure 4c) illustrates reflectivity >40 dBz extending 200 km from the vortex to a depth of 15 km, coincident with upper tropospheric O3 values <40 ppb (cf. Figure 2d). Patterns for other Caribbean hurricanes exceeding category 3 and tracking westward are similar and repetitious.
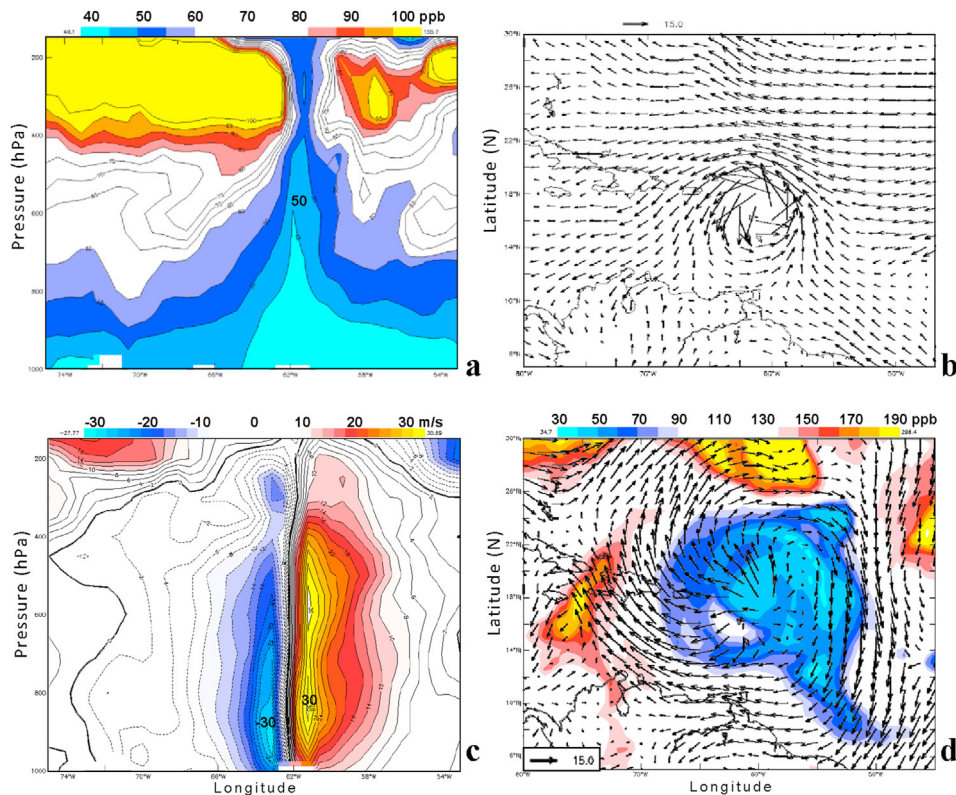


**Figure 2.** Hurricane Irma 6 Sep 2017 case study: (a) MERRA-2 ozone vertical section on 18N; (b) 925 hPa wind vector map, (c) meridional (V) wind section, and (d) 150 hPa wind vectors and ozone (shaded).
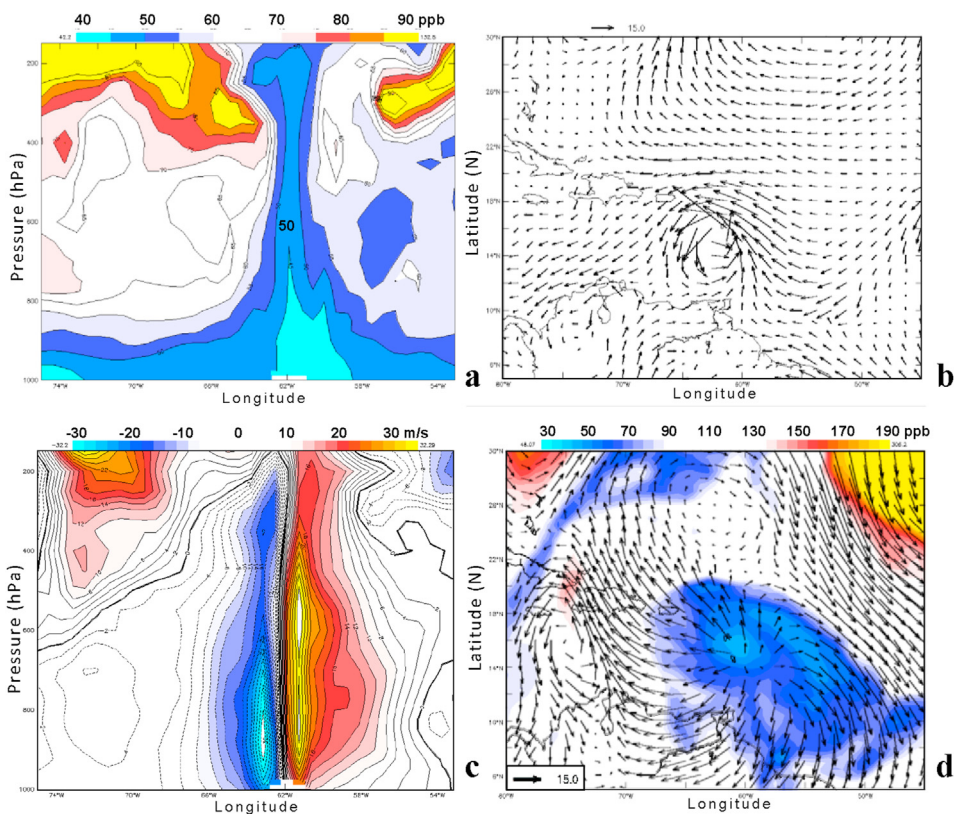
**Figure 3.** Hurricane Maria 19 Sep 2017 case study: (a) MERRA-2 ozone vertical section on 15N; (b) 925 hPa wind vector map, (c) meridional (V) wind section, and (d) 150 hPa wind vectors and ozone (shaded).
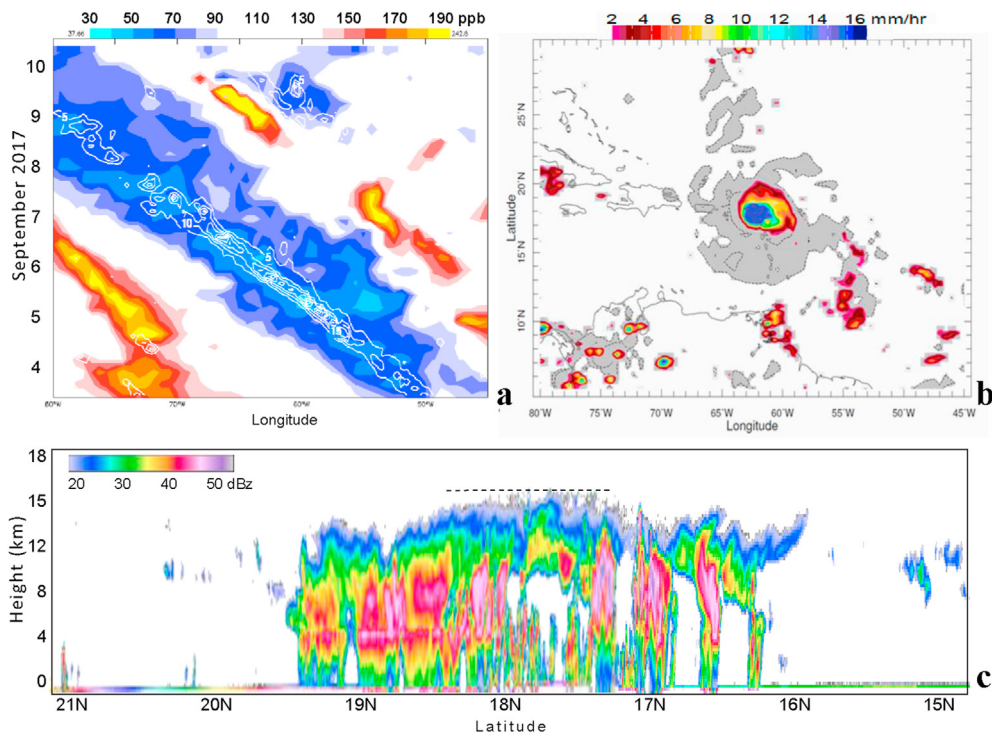


**Figure 4.** (a) Zonal propagation of 150 hPa ozone signal over a 7 day period along 18N in Irma case, with cMorph rain-rate white contours >5 mm/h. (b) Map of cMorph rain-rate (color-shaded >2 mm/h) and 500 hPa upward motion (grey-shaded < -.5 Pa/s) on 6 Sep 2017. (c) Cloudsat reflectivity section along 62W on 6 Sep 2017, dashed line is 150 hPa level.

## 5. Concluding discussion

Mean profiles of ozone over the tropical Atlantic (cf. Figure 1d) show a gradual rise of O3 concentration from 40 to 120 ppb from 1000 to 200 hPa. In the layer around 150 hPa (~14 km) ozone concentrations rise quickly, and are sensitive to vertical motions and measurement by satellite radiometers. The presence of a deep column of low ozone air depends on uplift via storm vorticity and associated convective heating. Vorticity translates into vertical motion (for TC with steady intensity and westward track) according to the simplified Eq. (1) derived from Holton (1992):

$$W = \xi \, (Z \, / \, f \, dt) \qquad \text{eq.1}$$

where $Z$ ~10 km depth, $f$ ~4.5 $10^{-5}$ s$^{-1}$, time scale (dt ~1 day). Using $\xi$ ~$10^{-4}$ s$^{-1}$ and other case values, the sustained mid-tropospheric uplift approaches 0.2 m/s. With upper divergence of similar magnitude (~$10^{-4}$ s$^{-1}$) upward motion reaches the 150 hPa level, bringing low ozone air (cf. Figures 2d, 3d). As TC eye-wall convection deepens, subsidence at distances >400 km from the core induce high ozone concentrations there. Past work has suggested that stratospheric intrusion of high ozone air is a common feature of TC (Das et al., 2016), but here the lifting of low ozone is more conspicuous and in agreement with Minschwaner et al. (2015).

Low ozone signatures around TC offer a powerful indicator of vortex interaction with the surrounding circulation and thermodynamic fields. The ozone cross-sections identify that intense TC have a deep column of low concentration. These may appear as a pyramid shape that is narrowed by intrusions of high ozone air on the leading edge (cf. Figure 3a, Irma). Hovmoller analysis of TC rainfall >5 mm/h cover a ~200 km swath consistent with the hurricane eye-wall and its convective heating. The evolution of upper tropospheric ozone concentrations <50 ppb delineate the radial extent of rising air in spiral bands, where moist air (CAPE >2000 J/kg) shields the inner core from dry air entrainment. Further work will compare model and satellite O3 fields, and study convective heating and vertical motion impacts on ozone fields around TC.

## 6. Summary and recommendations

In this research we have utlized upper level ozone as a tracer of vertical motion over Caribbean hurricanes. Storm organization and interaction with the surrounding circulation and thermodynamic features were evident in the results, which depend on data assimilated from multiple satellites especially designed for upper level ozone measurements. Hurricanes lift low ozone air from the marine layer, via vertical motions that can be traced to relative vorticity. Further work with tropical cyclones in other basins is underway, and appear to confirm our results from the Caribbean. It is believed that hurricane prediction will benefit from air chemistry data assimilation, not only for marine ozone but also for aerosol loading from terrestrial smoke and dust plumes.

## Declarations

### Author contribution statement

M. R. Jury: Analyzed and interpreted the data; Wrote the paper.

I. L. Fontanez-Vazquez: Conceived and designed the experiments; Wrote the paper.

### Funding statement

### Declaration of interests statement

The authors declare no conflict of interest.

### Additional information

No additional information is available for this paper.

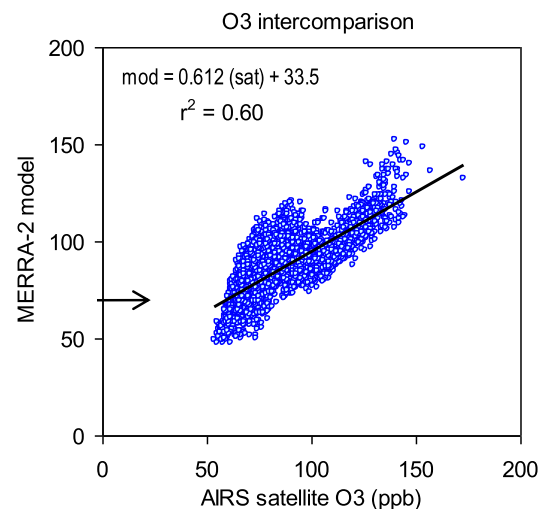### Acknowledgements

### Appendix



**Figure A1.** Intercomparison of satellite and model daily minimum 150 hPa O3 concentration in the eastern Caribbean 2005–2017, N = 4747. Cases listed in Table 2 are in the low end of the scatterplot (arrow).

### References

Boynard, A., Clerbaux, C., Coheur, P.-F., Hurtmans, D., Turquety, S., George, M., Hadji-Lazaro, J., Keim, C., Meyer-Arnek, J., 2009. Measurements of total and tropospheric ozone from IASI: comparison with correlative satellite, ground-based and ozonesonde observations. Atmos. Chem. Phys. 9, 6255–6271.

Cairo, F., 14 co-authors, 2008. Morphology of the tropopause layer and lower stratosphere above a tropical cyclone: a case study on cyclone Davina 1999. Atmos. Chem. Phys. 8, 3411–3426.

Cangialosi, J.P., Latto, A.S., Berg, R., 2018. Tropical Cyclone Report Hurricane Irma 30 Aug-12 Sep 2017. National Hurricane Center, Miami.

Carsey, T.P., Willoughby, H.E., 2005. Ozone measurements from eye-wall transects of two Atlantic tropical cyclones. Mon. Weather Rev. 133, 166–174.

Cuesta, J., et al., 2013. Satellite observation of lowermost tropospheric ozone by multispectral synergism of IASI thermal infrared and GOME-2 ultraviolet measurements over Europe. Atmos. Chem. Phys. 13, 9675–9693.

Das, S.S., Ratnam, M.V., Uma, K.N., Subrahmanyam, K.V., Girach, I.A., Patra, A.K., Aneesh, S., Suneeth, K.V., Kumar, K.K., Kesarkar, A.P., Sijikumar, S., Ramkumar, G., 2016. Influence of tropical cyclones on tropospheric ozone: possible implications. Atmos. Chem. Phys. 16, 4837–4847.

Gelaro, R., et al., 2017. The modern-era retrospective analysis for research and applications, MERRA-v2. J. Climate 30, 5419–5454.

Holton, J.R., 1992. An Introduction to Dynamic Meteorology. Academic Press, New York, p. 511.

Jang, K.I., Zou, X., DePondeca, M.S., Shapiro, M., Davis, C., Krueger, A., 2003. Incorporating TOMS ozone measurements into the prediction of the Washington, D.C., winter storm during 24–25 January 2000. J. Appl. Meteorol. 42, 797–812.

Jenkins, G.S., Robjhon, M.L., Reyes, A., Valentine, A., Nieves, L., 2015. Elevated middle and upper troposphere ozone observed downstream of Atlantic tropical cyclones. Atmos. Environ. 118, 70–86.

Joyce, R.J., Janowiak, J.E., Arkin, P.A., Xie, P.P., 2004. cMorph: a method that pro-duces global precipitation estimates from passive microwave and infrared data at high spatial and temporal resolution. J. Hydrometeorol. 5, 487–503.

Jury, M.R., 2016. Summer climate of Madagascar and monsoon pulsing of its vortex. Meteorol. Atmos. Phys. 128, 117–129.

Knowland, K.E., Ott, L.E., Duncan, B.N., Wargan, K., 2017. Stratospheric intrusion-influenced ozone air quality exceedances investigated in the NASA MERRA-2 reanalysis. Geophys. Res. Lett. 44, 10691–10701.

Langford, A.O., Masters, C.D., Proffitt, M.H., Hsie, E.-Y., Tuck, A.F., 1996. Ozone measurements in a tropopause fold associated with a cut-off low system. Geophys. Res. Lett. 23, 2501–2504.

Liu, Y., Zou, X., 2015. Impact of 4DVAR assimilation of AIRS total column ozone observations on the simulation of Hurricane Earl. J. Meteor. Res. 29, 257–271.

Liu, Y., Zhang, W., 2016. Improved hurricane forecasting from a variational bogus and ozone data assimilation scheme: case study. Meteorol. Atmos. Phys. 128, 715–732.

Logan, J.A., 1999. An analysis of ozonesonde data for the troposphere: recommendations for testing 3-D models and development of a gridded climatology for tropospheric ozone. J. Geophys. Res. 104, 16115–16149.

McPeters, R.D., Labow, G.J., Logan, J.A., 2007. Ozone climatological profiles for satellite retrieval algorithms. J. Geophys. Res. 112, D05308.

Minschwaner, K., Manney, G.L., Petropavlovskikh, I., Torres, L.A., Lawrence, Z.D., Sutherland, B., Thompson, A.M., Johnson, B.J., Butterfield, Z., Dubey, M.K., Froidevaux, L., Lambert, A., Read, W.G., Schwartz, M.J., 2015. Signature of a tropical Pacific cyclone in the composition of the upper troposphere over Socorro NM. Geophys. Res. Lett. 42, 9530–9537.

Molod, A., Takacs, L., Suarez, M., Bacmeister, J., 2015. Development of the GEOS-5 atmospheric general circulation model: evolution from MERRA to MERRA2, Geosci. Model Dev. 8, 1339–1356.

Monahan, K.P., Pan, L.L., McDonald, A.J., Bodeker, G.E., Wei, J., George, S.E., Barnet, C.D., Maddy, E., 2007. Validation of AIRS v4 ozone profiles in the UTLS using ozonesondes from Lauder, NZ and Boulder, USA. J. Geophys. Res. 112, D17304.

Orbe, C., Oman, L.D., Strahan, S.E., Waugh, D.W., Pawson, S., Takacs, L.L., Molod, A.M., 2017. Large-scale atmospheric transport in GEOS replay simulations. J. Adv. Mod. Earth Sys. 9.

Pasch, R.J., Penny, A.B., Berg, R., 2018. Tropical Cyclone Report, Hurricane Maria 2017. National Hurricane Center, Miami, p. 48.

Pittman, J.V., Pan, L.L., Wei, J.C., Irion, F.W., Liu, X., Maddy, E.S., Barnet, C.D., Chance, K., Gao, R.-S., 2009. Evaluation of AIRS, IASI, and OMI ozone profile retrievals in the extratropical tropopause region using in situ aircraft measurements. J. Geophys. Res. 114, D24109.

Prather, M.J., Ehhalt, D., 2001. Chapter 4: atmospheric chemistry and greenhouse gases. In: Climate Change 2001: the Science of Climate Change, Intergovernmental Panel on Climate Change. Cambridge University Press.

Read, K.A., 15 co-authors, 2008. Extensive halogen-mediated ozone destruction over the tropical Atlantic Ocean. Nature Lett. 453, 1232–1235.

Reid, P.C., 31 co-authors, 2009. Impacts of the oceans on climate change. Adv. Mar. Biol. 56, 1–150.

Ryu, J.-H., Jenkins, G.S., 2005. Lightning-tropospheric ozone connections: EOF analysis of TCO and lightning data. Atmos. Environ. 39, 5799–5805.

Saiz-Lopez, A., Fernandez, R.P., 2016. On the formation of tropical rings of atomic halogens: causes and implications. Geophys. Res. Lett. 43, 2928–2935.

Wargan, K., Labow, G., Frith, S., Pawson, S., Livesey, N., Partyka, G., 2017. Evaluation of the ozone fields in NASA's MERRA-2 reanalysis. NASA Manuscript 8, 2961–2988.

Wu, Y., Zou, X., 2008. Numerical test of a simple approach for using TOMS total ozone data in hurricane environment. Qtr. J. Roy. Meteor. Soc. 134, 1397–1408.

Zhang, L., Jacob, D.J., Liu, X., Logan, J.A., Chance, K., Eldering, A., Bojkov, B.R., 2010. Intercomparison methods for satellite measurements of atmospheric composition: application to tropospheric ozone from TES and OMI. Atmos. Chem. Phys. 10, 4725–4739.

Ziemke, J.R., Chandra, S., Duncan, B.N., Froidevaux, L., Bhartia, P.K., Levelt, P.F., Waters, J.W., 2006. Tropospheric ozone determined from Aura OMI and MLS: evaluation of measurements and comparison with the GMI Chemical transport model. J. Geophys. Res. 111, D19303.

Ziemke, J.R., Oman, L.D., Strode, S.A., Douglass, A.R., Olsen, M.A., McPeters, R.D., Bhartia, P.K., Froidevaux, L., Labow, G.J., Witte, J.C., Thompson, A.M., Haffner, D.P., Kramarova, N.A., Frith, S.M., Huang, L.-K., Jaross, G.R., Seftor, C.J., Deland, M.T., Taylor, S.L., 2019. Trends in global tropospheric ozone inferred from a composite record of TOMS/OMI/MLS/OMPS satellite measurements and the MERRA-2 GMI simulation. Atmos. Chem. Phys. 19, 3257–3269.

Zou, X., Wu, Y., 2005. On the relationship between total ozone mapping spectrometer ozone and hurricanes. J. Geophys. Res. 110, D06109.